Enhancement the perpendicular magnetic anisotropy of nanopatterned hard/soft bilayer magnetic antidot arrays for spintronic application

M. Salaheldeen[1, 2*], L. Martínez-Goyeneche[2], P. Álvarez-Alonso[2], A. Fernández[2]

1) Physics Department, Faculty of Science, Sohag University, 82524 Sohag, Egypt
2) Depto. Física, Universidad de Oviedo, C/ Federico García Lorca 18, 33007 Oviedo, Asturias, Spain

Abstract:

Development of perpendicular magnetic anisotropy (PMA) thin films is a requisite for many applications. In this work, we have illustrated the enhancement of the PMA of Hard (Co)/ Soft (Permalloy, Py) ferromagnetic bilayers by depositing them onto nanoporous anodic alumina membranes with different hole diameters varying in the range between 30 nm and 95 nm. A dramatic change in the hysteresis loops behaviour with hole size, D, and magnetic surface cover ratio parameters has been observed: (1) for samples with small antidot hole diameters, the in-plane (INP) hysteresis loops show single-step magnetic behaviour; (2) for D = 75 nm, the hysteresis loops of Co/Py and Py samples exhibit a multistep magnetic behaviour; (3) a decreasing coercivity in the INP hysteresis loops for antidot arrays samples with D > 75 nm has been detected as a consequence of the reduction of the in-plane magnetic anisotropy and the rising of the out-of-plane component. A crossover of magnetic anisotropy from the in-plane to out-of-plane for bilayer antidot samples has been observed for Co/Py ferromagnetic bilayers, favoured by the interfacial exchange coupling between the two ferromagnetic materials. These findings can be of high interest for the development of novel magnetic sensors and for perpendicular-magnetic recording patterned media based on template-assisted deposition techniques.

Keywords; Structured magnetic thin films, magnetic antidot arrays, magneto-optic Kerr effect, perpendicular magnetic anisotropy, spintronics.

Introduction:

Recently, thin film heterostructures that consist of hard magnetic anisotropy layers coupled with soft magnetic layers (hard/soft bilayer exchange coupling) have been widely studied because of their potential for perpendicular magnetic recording media [1], spin-transfer torque switching [2], and nano-oscillator devices [3]. It has been reported that the exchange interaction and the spin-orbit interaction between hard and soft magnetic phases lead to a significant modification of the magnetization reversal mechanism and an enhanced perpendicular magnetic anisotropy [1,4].

The inclusion of artificial defects in the bilayers thin film has been demonstrated as a powerful approach to engineer their magnetic properties in multiple ways. In particular, the antidot arrays nanostructured thin films represent nowadays an important tool for modifying the static and dynamic magnetic properties of host material by changing its geometrical parameters [5–7]. In this regard, it has been recently found that the magnetic anisotropy can be reoriented from in-plane to out-of-plane by only modifying the hole size for a single layer of ferromagnetic materials [6,8]. The existence of arrays of nanoholes can induce a demagnetization field distribution, which modifies the magnetic properties of the nonpattern thin films such as its magnetization reversal mechanism, the coercive field, and the intrinsic magnetic anisotropy [9]. The ability to control the strength and orientation of magnetic anisotropy becomes essential in advanced applications such as innovative electronic devices [10], spintronic devices [11], or perpendicular bit pattern magnetic recording media [12], especially for improving the thermal stability and switching reliability of magnetic bits [8].

In this work, we pay special attention to the enhancement of the perpendicular magnetic anisotropy of Co/Py bilayers antidot arrays by studying the effect of the geometrical parameters, namely shape and size of nanohole on their magnetic properties. The effect of layer thickness in the magnetic anisotropy of Co/Py bilayer thin film has been studied by Béron et al. [20]; they concluded that the thinner Co/Py (15 nm) induced a localized perpendicular anisotropy, meanwhile the thicker samples do not show such localized perpendicular magnetic anisotropy around the nanoholes. Therefore, we focus our study on the effect of antidot hole diameter on the magnetic anisotropy of the Co/Py bilayer antidot arrays samples with layer thickness 15 nm. In addition, we study the same parameters for Co and Py single layer for better comparison and understanding.

Materials and methods

The pre-patterned masks for the Co, Py, and Co/Py bilayers antidot arrays, consisting of hexagonally ordered nanoporous alumina membranes, were produced through the conventional two-step mild anodization process [13,14]. High purity Al foils (99.999 %) with a 0.5 mm thickness and area (1.5×1.5 cm^2) was electropolished with a mixture of H_3PO_4 and H_2SO_4 to improve the surface smoothness. These Al foils were cleaned and electropolished at 50 V in perchloric acid and ethanol solution (1:3 vol., 9 °C) for 8 min, then the two-step electrochemical anodization was carried out as described elsewhere [14]. During the 2nd anodization step, which lasted for 5 h, the nanopores grew following the highly self-ordered hexagonal symmetry pre-patterned engineering during the first anodization process. To obtain the porous anodic alumina, PAA, templates with different pore size, the masks were chemically etched in 6 wt.% orthophosphoric acid at 40 °C for different etching times, $\boldsymbol{T_{etching}}$, between 25 and 75 minutes. This technique allowed us to obtain a series of PAA templates with a wide range of different pore diameters, **Dp**, varying between 34 ± 3 to 96 ± 3 nm but keeping constant the interpore distance, ***P***, to the value of 105 ± 4 nm and hole depth around 40 mm, as listed in table 1.

Antidot and continuous thin films samples were deposited onto PAA templates and 0.5 mm thick glass substrates at room temperature by means of the ultra-high vacuum thermal evaporation technique using an E306A thermal vacuum coating unit (Edwards, Crawleyx), respectively, with an ultimate vacuum around 3.7×10^{-7} mbar (see [6,15] for details). Metallic Al, Co, Ni, and Fe targets were used as source materials (purity 99.99%). Co-deposition of Fe and Ni resulted in the deposition of $Fe_{21}Ni_{79}$ (Permalloy) thin films, as determined by the EDX measurements carried out in a MEB JEOL-6610LV scanning electron microscopy (SEM). The control of the film thickness was achieved by using two independent quartz crystal controllers that monitored simultaneously the deposition rates of each evaporation source [15]. The layer thickness of Co and Py samples is 10 nm and 5 nm respectively; Co/Py bilayers were deposited with the same layer thickness (total thickness of the magnetic materials is 15 nm). The continuous Co, Py, and Co/Py bilayer thin films were also deposited with the same thicknesses as for the antidots samples to compare the magnetic properties. All specimens were covered with a capping Al film (3 nm) to avoid the oxidation. The chemical composition of Co/Py bilayer antidot arrays thin films was confirmed with EDX, as indicated in the figure 1.

The surface magneto-optic properties of the antidot array and continuous layers were measured making use of a scanning laser Magneto-Optical Kerr Effect (MOKE) magnetometer set up; details of measurements are reported elsewhere [6,8,15]. The measurements have been done at room temperature in a direction parallel to the film plane (In-Plane, INP) using transversal MOKE. Complementary bulk magnetic measurements of Co, Py, and Co/Py bilayer antidot array thin films and their corresponding non-pattern thin films were carried out by using a vibrating sample magnetometer, VSM, with applied magnetic fields up to ± 2 T, measured at room temperature and in both in-plane and out-of-plane directions to the film plane, respectively.

Results and discussion

After the thermal layer evaporation process, all samples have been analysed by SEM to measure the nanohole diameter, the magnetic cover ratio, and the edge-to-edge distance, as summarized in table 2. Figure 2(a) shows the top view image Co/Py bilayer continuous thin films with thickness 15 nm, while five selected images of Co/Py bilayer antidot samples having different hole diameters values are plotted in figure 2(b-f). For all antidot samples, well-ordered hexagonal arrangements of nanoholes with a constant lattice parameter $P \sim 105 \pm 4$ nm have been observed, in good agreement with what is commonly obtained in the patterned alumina substrate after the two-step anodizing procedure in 0.3M Oxalic acid at 50 V [14,16].

Table 1. Pore diameter D_p, the centre-centre distance P, and edge-to-edge separation W ($W = P - D_p$) of the nanoporous alumina templates as a function of the time etching.

Time etching (min)	Pore diameter (Dp) nm	centre-centre distance P (nm)	Edge-to-edge separation W = P- Dp (nm)
25	34 ± 3	107 ± 2	73 ± 3
34	64 ± 3	104 ± 5	40 ± 3
48	78 ± 2	102 ± 3	24 ± 3
65	87 ± 4	108 ± 2	23 ± 3
75	96 ± 3	107 ± 3	11 ± 3

The magnetic surface coverage ratio, C, is a parameter that describes the amount of the magnetic materials for each antidot arrays sample and is usually estimated by the following relation [17]:

$$C = 1 - \frac{\pi D^2}{2\sqrt{3}\,P^2} * 100 \qquad (1)$$

The values derived from equation (1) for Co, Py, and Co/Py bilayer antidot arrays samples with different geometric parameters (hole diameter, centre- centre distance and edge-to-edge separation) are summarized in table 2. The lowest value of the magnetic surface coverage ratio about 28.5-31.4 % has been obtained for Co, Py, and Co/Py bilayer antidot arrays samples with hole diameter 93 nm, 94 nm, and 95 nm, respectively, and interhole distance P =107 ± 3 nm, being lower than the ones reported in ref. [18–20]. The wide variation of hole diameter, **W**, and **C** has enabled us to study the full possible geometric parameters of Co, Py, and Co/Py bilayer antidot films deposited on nanoporous alumina membrane and their effect on the magnetic properties, especially the magnetic anisotropy.

Table 2. The geometrical parameters and magnetic surface coverage ratio percentage, C, of Co, Py, and Co/Py antidot arrays thin film with different hole diameter, D, and their corresponding non-pattern samples.

	Co			Py			Co/Py		
Sample	~D (nm)	~C %	~W (nm)	~D (nm)	~C %	~W (nm)	~D (nm)	~C %	~W (nm)
S_{TF}	-	100	-	-	100	-	-	100	-
S1	30 ± 2	92.9	77 ± 2	31 ± 3	92.4	76 ± 3	32 ± 1	92.0	75 ± 2
S2	60 ± 3	69.8	44 ± 3	59 ± 1	70.8	45 ± 4	61 ± 3	69.0	43 ± 4

S3	74 ± 2	52.2	28 ± 3	74 ± 2	52.2	28 ± 2	75 ± 3	51.0	27 ± 3
S4	84 ± 3	45.1	24 ± 4	83 ± 3	46.4	25 ± 4	85 ± 3	43.8	23 ± 2
S5	93 ± 3	31.4	14 ± 3	94 ± 4	30.0	13 ± 3	95 ± 3	28.5	12 ± 2

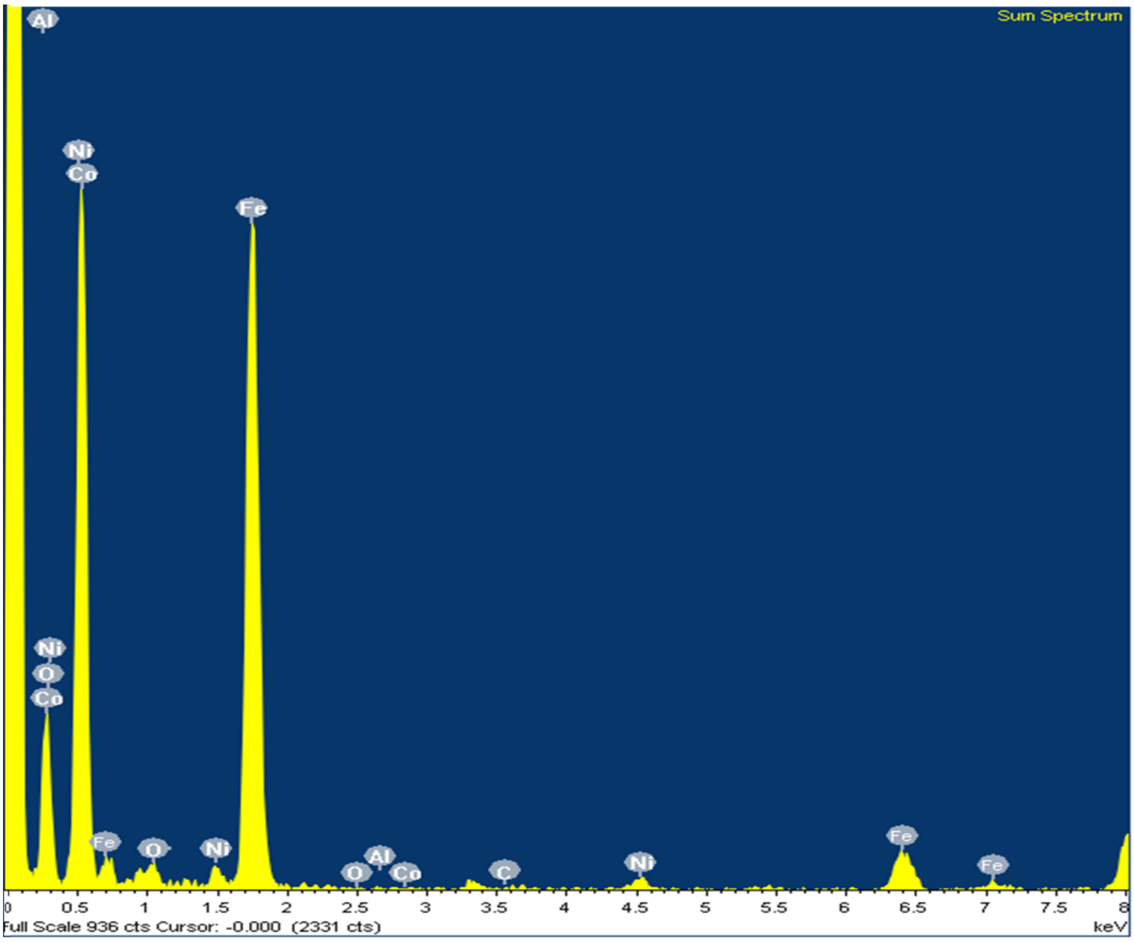

Figure 1. The EDX spectrum analysis of Co/Py bilayer antidot arrays thin films that proves the existence of Co and Py elements. The presence of Al and O_2 in the spectrum comes from the nanoporous alumina template and the capped layer of samples.

Figure 3 shows representative INP MOKE hysteresis loops of Co (15 nm), NiFe (Py) (15 nm), and Co (10 nm)/Py (5 nm) antidot arrays thin films with different geometric parameters, i.e., different magnetic cover ratio percentage, with labels **S1**, **S2**, **S4**, and **S5**, as listed in table 2. In addition, the corresponding unpatterned thin films of the same thickness have been employed as a reference and labelled as $\mathbf{S_{TF}}$. In previous studies about magnetic antidot arrays thin films, a striking increase of INP coercivity, $H_{C//}$, with respect to the non-patterned thin films is commonly reported from a few Oe to several tens of Oe, depending on the material, magnetic surface coverage ratio, and relative orientation of the magnetic field and the magnetic anisotropy easy axis [6,17]. In our current study, the maximum INP coercivity has raised by a factor of 22 for Py antidot arrays with label **S3** compared to the non-patterned thin films, and it is 7 times larger for **S4** and **S3** Co and Co/Py bilayer antidot samples, respectively, compared to their corresponding reference samples $\mathbf{S_{TF}}$. Besides, several differences have been found in the INP magnetic properties of Co, Py, and Co/Py bilayer antidots when compared to their corresponding continuous thin films. Firstly, the INP hysteresis loop loses its squareness, especially for samples **S2** to **S5** for all antidot samples. Secondly, a light multistep magnetization behaviour has been observed for **S3** Py and **S3** and **S5** Co/Py bilayer antidot samples, as shown in figure 3. This multistep magnetic behaviour in **S3** Py specimen is characteristic of a contribution of the OOP magnetic anisotropy component that comes from the magnetic signal of the inner wall of nanoholes (see figure 2(h)) and the strong interfacial exchange coupling between the two ferromagnetic materials, as reported in [6,8,21–23]. For the Co/Py specimens, it is also present a hard/soft interfacial coupling accompanied by a complex magnetization reversal process and a strong pinning of magnetic domains wall movement [4,23,24]. Meanwhile, the hysteresis loops of Py and Co/Py bilayer antidot samples with the smallest hole size -equivalently, the highest magnetic surface coverage ratio- and Co antidot samples exhibit a single-step magnetization process, as shown in figure 3. Therefore, the geometric parameters of nanoporous alumina and the hosting magnetic materials can play an effective role in tailoring the magnetization reversal process.

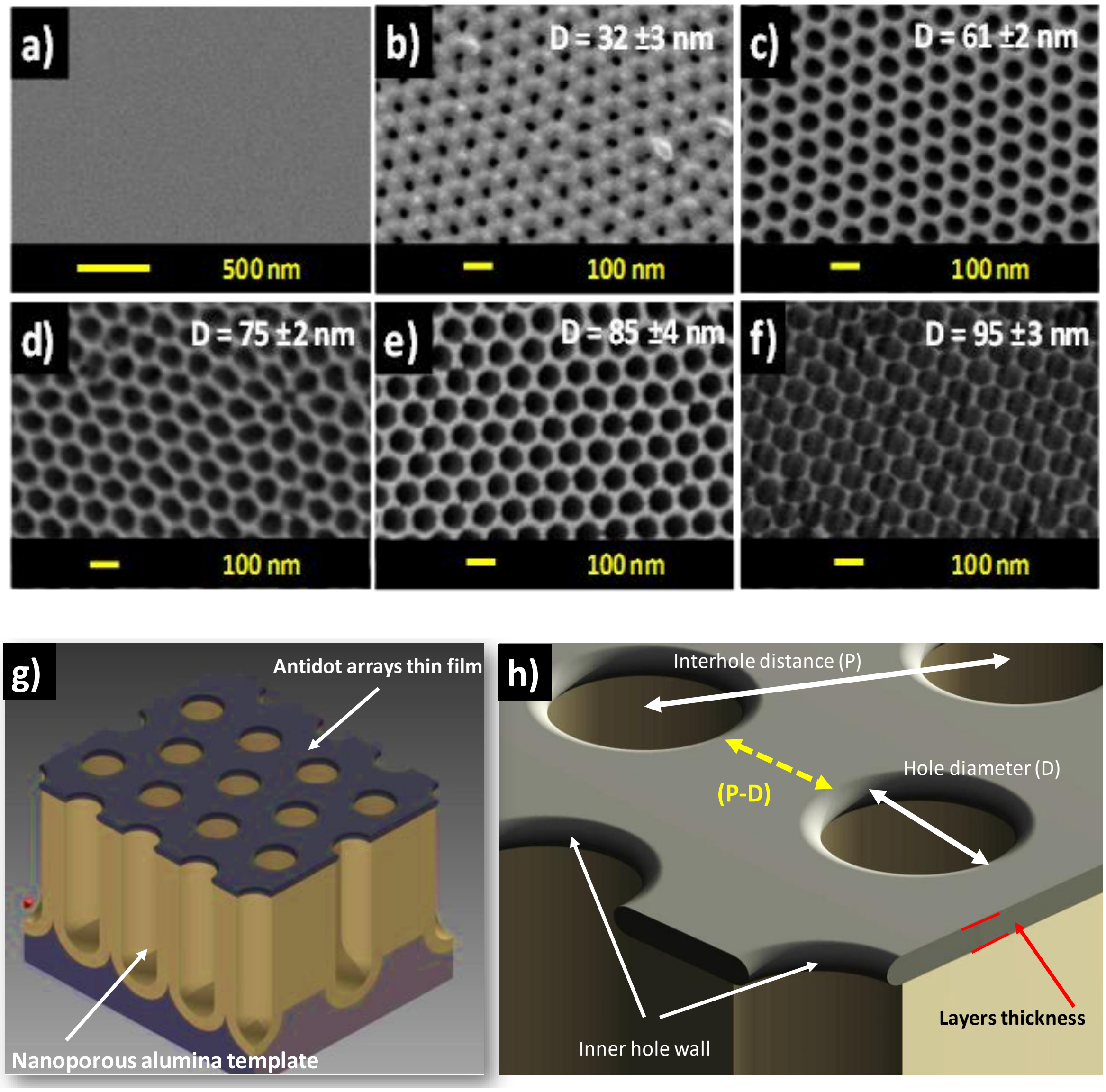

Figure 2. (a−f) SEM images of the Co/Py bilayer deposited on the top surface of (a) glass substrate to obtain the continuous thin films samples as a reference, and (b-f) on the top surface of the PAA templates after being submitted to the pore widening process under different chemical etching times. (g) and (h) represent the 3D sketch of antidot arrays thin films, which illustrates the geometrical parameters on top of nanoporous alumina template.

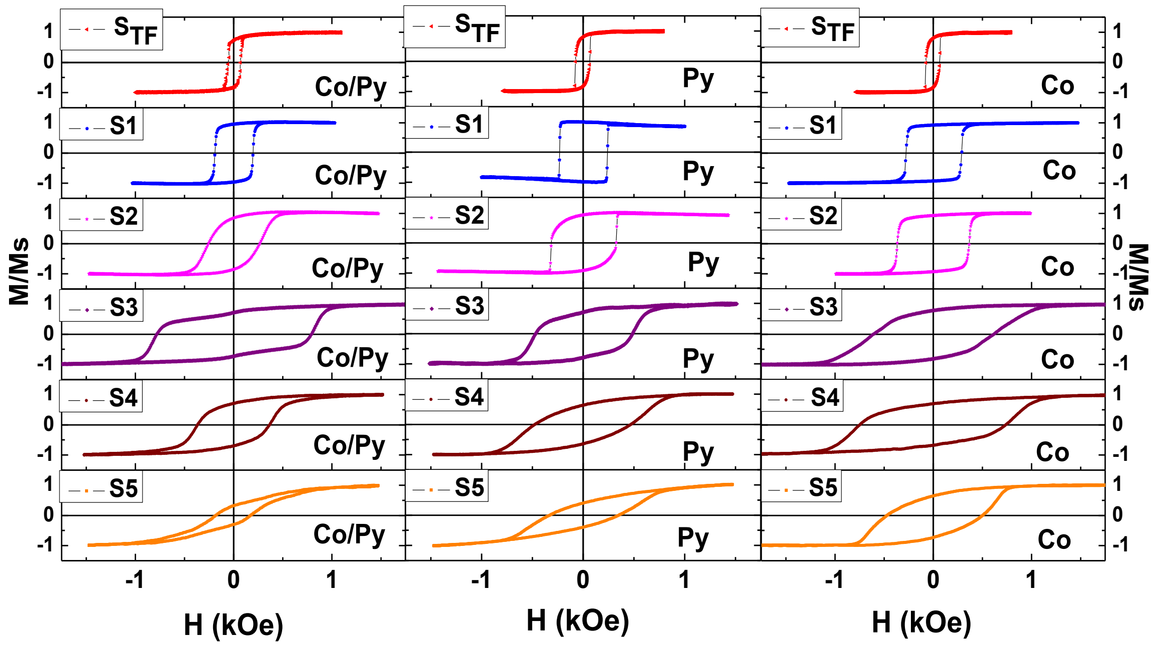

Figure 3. In-plane transversal MOKE hysteresis loops of Co/Py bilayer antidot arrays and corresponding non-patterned film, S_{TF}. The layer thickness of magnetic materials for all samples is fixed at 15 nm.

Figure 4 summarises the estimation of in-plane coercivity, $H_{C//}$, and the reduced in-plane remanence, $m_{r//}$, of Co, Py, and Co/Py bilayer antidot arrays thin films with respect to the hole diameter. $H_{C//}$ and $m_{r//}$ present a dramatic change with D. First, the monotonic $H_{C//}$ increment with the hole diameter values reaches the maximum value for antidot samples with D ~75 nm (i.e., C ~ 52 % and W ~ 24 nm), being $H_{C//}$ = 578 Oe and 866 Oe for Py, and Co/Py bilayer antidot arrays thin films, respectively. Meanwhile, the maximum value of the $H_{C//}$ = 648 Oe for Co antidot arrays thin film has been detected for antidot samples with D ~ 84 nm (i.e., C ~ 45 % and W ~ 28 nm). Secondly, a further increase of D leads the $H_{C//}$ to decrease until reaching the minimum values of 400 Oe, 435 Oe, and 220 Oe for Co, Py, and Co/Py bilayer antidot arrays thin films, respectively, as indicated in figure

4(a). The Co and Py antidot arrays samples with D ~ 94 ± 1 nm (i.e., C ~ 30 ± 1 % and W ~ 13 ± 1 nm) show the minimum reduction of $H_{C//}$, as the difference between the highest and the lowest values of $H_{C//}$ are 178 Oe and 207 Oe for Co and Py antidot arrays samples, respectively; a similar behaviour has been observed for Co and Py antidot arrays thin films in a previous work but by using lithographic techniques [25]. Meanwhile, the reduction of $H_{C//}$ of Co/Py bilayer antidot samples is rapid, being the difference between the highest and the lowest values of $H_{C//}$ 646 Oe, i.e. more than 3 times that detected in single layer antidot samples. Therefore, an in-plane critical hole diameter, $D_{c//}$, has been supposed for Co, Py, and Co/Py bilayers antidot samples, where $H_{C//}$ starts to decrease with D increasing. For the reduced remanence behaviour with D, all antidot arrays samples show a noticeable decreasing of $m_{r//}$ with antidot hole diameter increment, as plotted in figure 4(b), where the $m_{r//}$ shows its maximum for non-pattern samples (**S_{TF}**) and the minimum for antidot arrays samples with the largest hole size. In fact, the reduction of $m_{r//}$ with the increase of D is related to the reduction of the edge-to-edge distance between two holes (i.e., the growth of antidot hole diameter), in which the magnetization component along the perpendicular direction to the sample surface becomes higher and stronger [23]. In addition, as W is further decreased, the inter distance between adjacent holes becomes narrower and the film area that is nucleated is very small, therefore the magnetization reversal is more favourable via the coherent rotation rather than domain wall movement, which may lead to a further decrease of $H_{C//}$ and $m_{r//}$ [8,25]. Due to the strong interfacial exchange coupling between the two ferromagnetic structures in Co/Py bilayers, the reduction of $H_{C//}$ and $m_{r//}$ is higher than the observed in the single magnetic layer thin films [22].

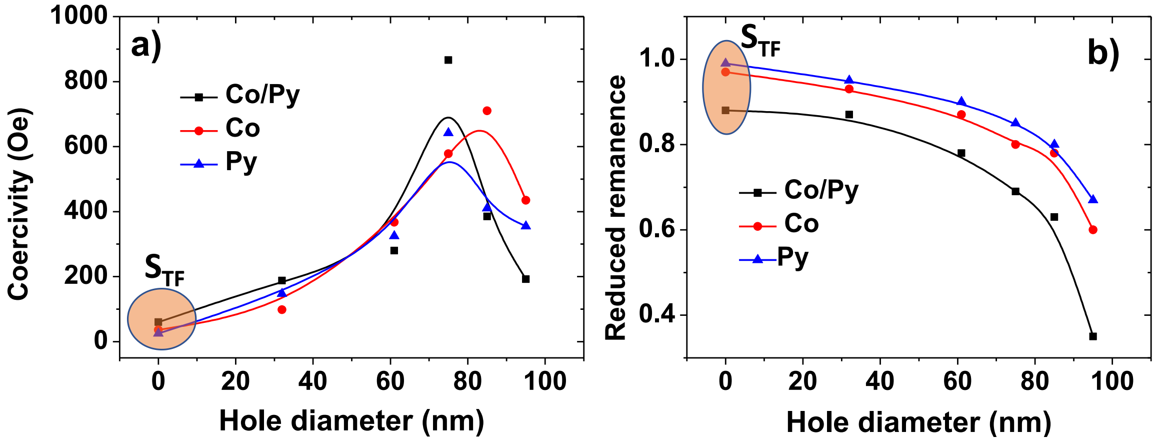

Figure 4. a) Coercivity and b) reduced remanence dependence for the INP directions of the Co, Py, and Co/Py bilayer antidot array samples as a function of (a) antidot hole.

To determine the effect of the antidot hole on the magnetic anisotropy easy axis direction in the Co/Py thin films, we have measured the INP and OOP loops for Co/Py bilayers antidots with hole diameter by using VSM magnetometer (see figure 5). For **S_{TF}**, **S1**, **S2**, and **S3** Co/Py bilayers samples, the magnetization is, initially, INP oriented, as indicated by the large $m_{r//}$ and large values of the coercivity. In contrast, we have detected a near-zero remanence magnetization and a high saturating magnetic field measured along the OOP orientation (Figure 5(a-d) red loop).

Regarding the INP coercive field, the antidot samples exhibit larger values comparing to the **S_{TF}**, which has been observed also in [8,24] and ascribed to the pinning effect of the holes. By increasing the antidot hole diameter, the in-plane coercivity increment reaches the maximum for **S3** antidot arrays samples, in concordance with the results obtained from MOKE measurements (see figure 3 and figure 5(d)). A sudden decrease in the in-plane magnetic coercivity and an increase in the out-of-plane coercivity have been observed for **S4** Co/Py bilayers antidots sample, as depicted in figure 3 and figure 5(e). The same behaviour has been detected for Co and Py single layer antidot arrays samples. Finally, a dominant magnetization component perpendicular to the plane of the sample surface has been detected only for **S5** Co/Py bilayers antidot arrays samples, as can be seen in figure 5(f). Meanwhile, the **S5** antidot samples of Co and Py have not shown a dominant perpendicular magnetic anisotropy. Therefore, the transition from the INP to OOP magnetic anisotropy for Co/Py bilayer antidot samples can be ascribed to a strong interfacial exchange coupling between the two FM materials. In fact, antidot thin films deposited on the top-surface of nanoporous alumina membrane templates reproduce the intrinsic surface roughness of the patterned templates [26,27] and develop a crescent shape during the thin film deposition process, as indicated at figure 2(h) and reported in ref. [6,21,23]. These two morphological features can determine the magnetic anisotropy of the material. In this regard, the magnetic moments between nanoholes remain aligned parallel within the film plane, while magnetic moments along the inner walls of the nanoholes of antidot films are perpendicularly aligned to the film plane [6,28]. The contribution of the magnetization component along the perpendicular direction to the sample surface becomes higher as the nanoholes diameter increases (i.e., magnetic surface coverage decreases) [19], but the magnetostatic energy associated with the antidot array raises with the antidot hole diameter. Therefore, when the hole diameter is large enough to counterbalance the energy associated with the magnetic poles on the film surface, the preferred direction of magnetization should change from the INP to the OOP direction, as detected in Co/Py bilayers antidot arrays thin films and also reported for magnetic antidot arrays thin films with large hole diameter [6,12,15].

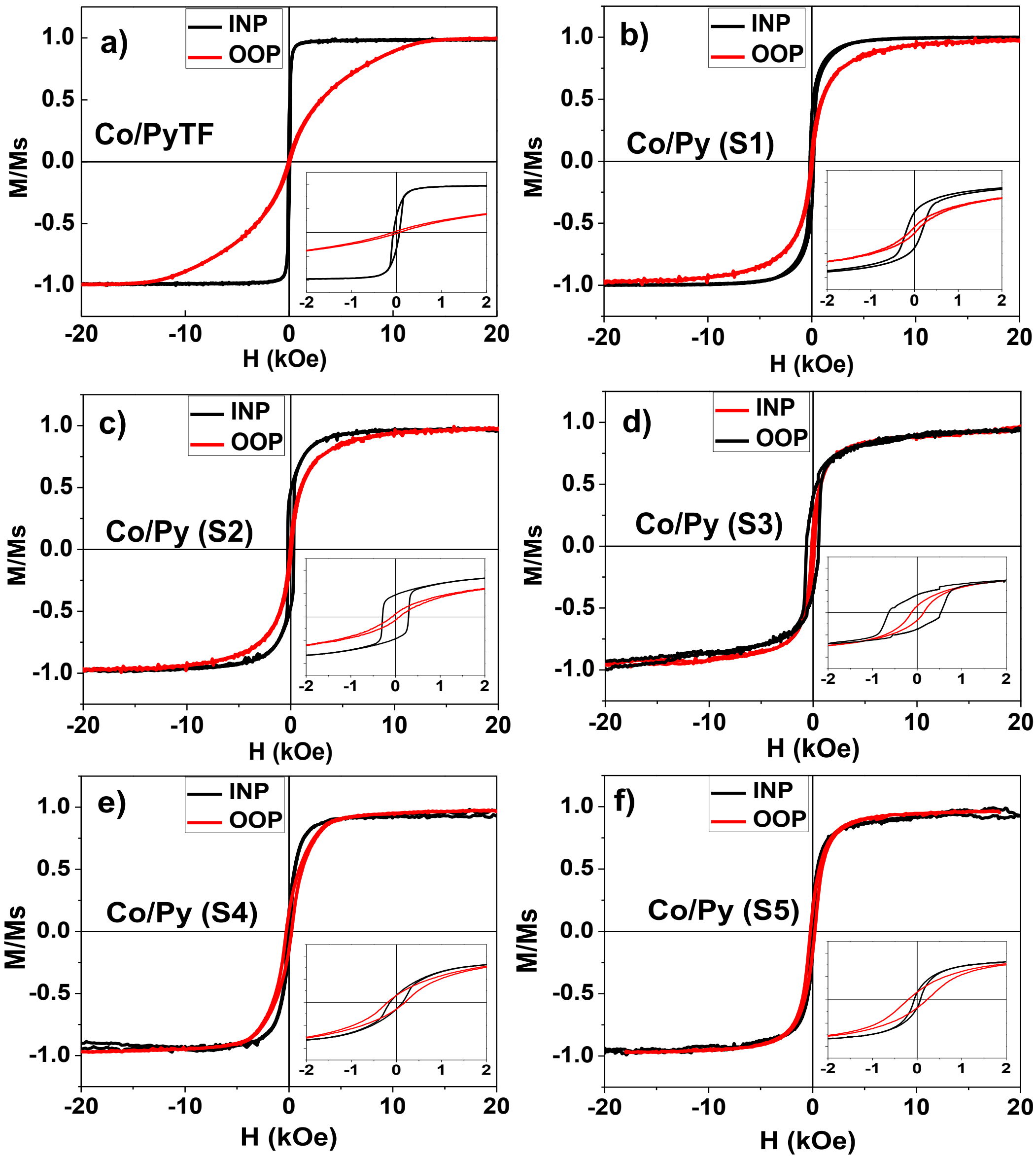

Figure 5. The INP (black color) and OOP (red color) VSM hysteresis loops of Co/Py bilayer a) for continuous thin film and b) to f) antidot arrays thin films with a 15 nm layer thickness and different hole diameters. Insert the low scale magnetic field from 2 kOe to -2 kOe loops.

By analysing the INP and OOP loops we can estimate the effective magnetic anisotropy coefficient, K_{eff} -which represents an important parameter in spintronic application- as a function of the size of holes diameter variation. The effective magnetic anisotropy is determined from the difference between the areas of the INP and OOP hysteresis loops and can be calculated by the given expression [12,29]:

$$\boldsymbol{K_{eff}} = K_{(\mathrm{OOP})} - K_{(\mathrm{INP})} = \int_{0-\mathrm{OOP}}^{M_s} (H\mathrm{d}M) - \int_{0-\mathrm{INP}}^{M_s} (H\mathrm{d}M) \tag{2}$$

where M is the magnetization, M_S represents the saturation magnetization, and H is the applied magnetic field. A noticeable tendency of $\boldsymbol{K_{eff}}$ depending on the antidot hole diameter can be observed in figure 6; the larger the INP magnetic surface coverage ratio (i.e., $\mathbf{S_{TF}}$ and antidot with small $\boldsymbol{D}$), the greater the effective magnetic anisotropy coefficient. This trend can be explained by a model based on the influence of nanoholes edge defects, which reduces the value of the INP magnetic anisotropy locally [6,30,31]. The Co, Py, and Co/Py thin film $\mathbf{S_{TF}}$ samples show an INP effective magnetic anisotropy that is mainly due to the shape anisotropy of the sample. For all antidot arrays samples, the INP $\boldsymbol{K_{eff}}$ decreases with the increment of antidot hole diameter, which means that the hard magnetization axis displayed by the continuous unpatterned thin film, pointing along the out-of-plane direction, becomes softer for the antidot samples with larger holes diameter [29,32]. Moreover, a dramatic change in the easy magnetization axis of the Co/Py bilayers antidot arrays sample occurs when the nanohole diameter crossed above its critical size (for a determined value of D ≈ 85 nm), rotating from the INP direction (positive values of $\boldsymbol{K_{eff}}$) toward OOP direction (negative values of $\boldsymbol{K_{eff}}$), when the value of nanoholes diameter equals 94 nm [23,33]. Such a crossover of magnetization from INP toward OOP direction has not been detected for Co and Py antidot arrays samples, which suggests that the strong coupling between two ferromagnetic elements plays a key role in inducing the perpendicular anisotropy. Such enhancement of the PMA in Co/Py bilayer antidot array structures opens an interesting route for these materials as promising candidates for spin transfer torque magnetic random-access memories (STTMRAM) and perpendicular bit patterned magnetic storage media applications [31,32].

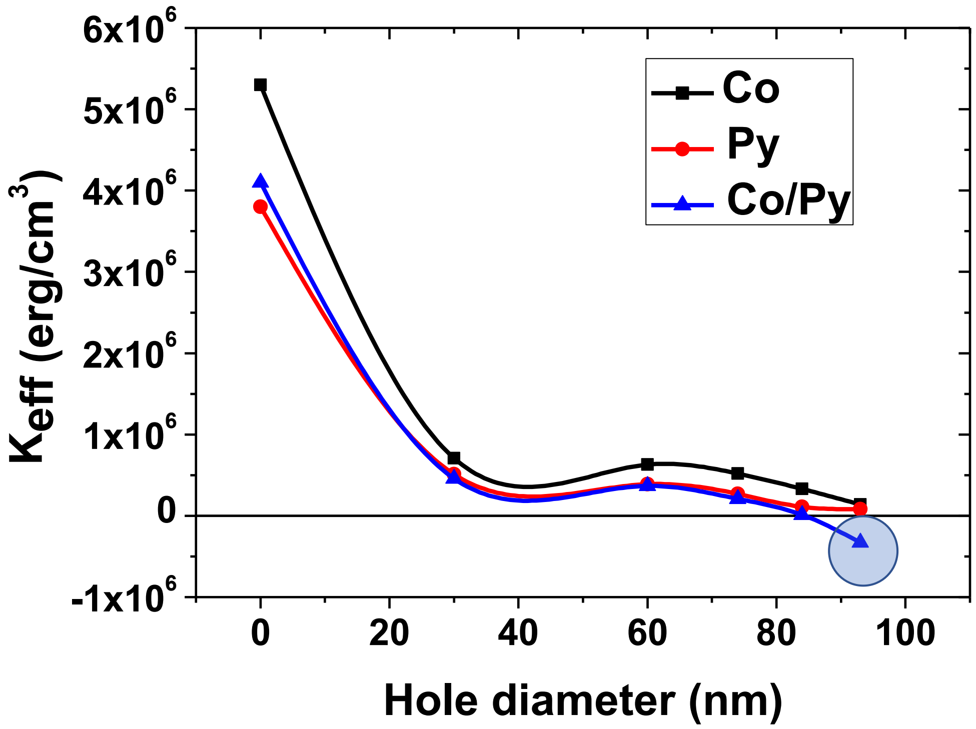

Figure 6. Effective anisotropy, $\boldsymbol{K_{eff}}$, as a function of antidot hole diameter for Co, Py, and Co/Py bilayers antidot thin films. Negative values of $\boldsymbol{K_{eff}}$ correspond to antidot samples with perpendicular (OOP) effective anisotropy.

Conclusions

The magnetic properties of Co, Py, and Co/Py bilayer antidot arrays thin films are strongly dependent on the geometrical parameters of nanoporous alumina template. All antidot arrays samples exhibit a sharp increase in the coercivity compared to non-pattern films due to the strong pinning effect induced by the nanoholes. A dramatic change in the in-plane coercivity of all antidot arrays samples with variation the magnetic surface coverage ratio has been detected. Initially, the $H_{C//}$ monotonically increases with increasing hole diameter up to D ≈ 75 nm, then decreases with further increment of D. In addition, the in-plane hysteresis loops for $\mathbf{S_{TF}}$ and samples with small hole diameter show single step magnetic behaviour, meanwhile the in-plane loops of Py and Co/Py bilayers samples with D ≈ 75 nm show multi-step magnetic behaviour due to the strong contribution of out-of-plane magnetic component that comes from the inner wall of the nanohole. Special attention must be paid to the Co/Py bilayers antidot arrays samples, as they exhibit the capacity to transfer the magnetization from the in-plane easy axis (Co/Py bilayer non-pattern thin films) to out-of-plane easy magnetization axis (Co/Py bilayer antidot samples with D = 95 nm), mainly due to the interfacial exchange coupling between the two ferromagnetic materials. In contrast, the strong in-plane magnetic anisotropy for the single ferromagnetic antidot samples, especially for Co antidot arrays samples, would shift the magnetic crossover away from our experimental limits. The highest value of the effective perpendicular magnetic anisotropy observed for the Co/Py bilayers antidot thin film with D = 95 nm make them excellent candidates for spintronics applications, bit patterned magneto-optic perpendicular recording media, and magnetic sensors based on template assisted deposition methods. Finally, the dual behaviour of INP/OOP coercivity points towards a new nanotechnological strategy of fabrication arrays of magnetic bits, i.e., basic elements for magneto-optic perpendicular recording patterned media, embedded into a 2D structural system.

Acknowledgment

This work has been financially supported by Spanish MCIU and AEI and European FEDER (MCIU-19-RTI2018-094683-B-C52), and Principado de Asturias (IDI/2018/000185), Spain. Authors are also indebted to Dr. C. Quirós from CINN (CSIC—Univ. de Oviedo) and Eng. M. Hassan from (Nanomembrane-Egypt) and D. Martínez Blanco and A.J. Quintana García from scientific and technological resources of the University of Oviedo for the technical support given.

References:

[1] Andrieu S, Hauet T, Gottwald M, Rajanikanth A, Calmels L, Bataille A M, Montaigne F, Mangin S, Otero E, Ohresser P, Le Fèvre P, Bertran F, Resta A, Vlad A, Coati A and Garreau Y 2018 Co/Ni multilayers for spintronics: High spin polarization and tunable magnetic anisotropy *Phys. Rev. Mater.* **2** 064410

[2] Choi G M, Schleife A and Cahill D G 2017 Optical-helicity-driven magnetization dynamics in metallic ferromagnets *Nat. Commun.* **8** 15085

[3] Haidar M, Awad A A, Dvornik M, Khymyn R, Houshang A and Åkerman J 2019 A single layer spin-orbit torque nano-oscillator *Nat. Commun.* **10** 2362

[4] Deng J X, Tan A, Li J, Hwang C and Qiu Z Q 2016 In-plane spin reorientation transition in Co/Py bilayers grown epitaxially on vicinal Cu(001) *J. Magn. Magn. Mater.* **408** 193–8

[5] Tse D H Y, Steinmuller S J, Trypiniotis T, Anderson D, Jones G A C, Bland J A C and Barnes C H W 2009 Static and dynamic magnetic properties of Ni80 Fe20 square antidot arrays *Phys. Rev. B - Condens. Matter Mater. Phys.* **79** 054426

[6] Salaheldeen M, Méndez M, Vega V, Fernández A and Prida V M 2019 Tuning Nanohole Sizes in Ni Hexagonal Antidot Arrays: Large Perpendicular Magnetic Anisotropy for Spintronic Applications *ACS Appl. Nano Mater.* **2** 1866–1875

[7] Ding J and Adeyeye A O 2013 Binary ferromagnetic nanostructures: Fabrication, static and dynamic properties *Adv. Funct. Mater.* **23** 1684–91

[8] Salaheldeen M, Vega V, Fernández A and Prida V M 2019 Anomalous in-plane coercivity behaviour in hexagonal arrangements of ferromagnetic antidot thin films *J. Magn. Magn. Mater.* **491** 165572

[9] Cowburn R P, Adeyeye A O and Bland J A C 1997 Magnetic domain formation in lithographically defined antidot Permalloy arrays *Appl. Phys. Lett.* **70** 2309

[10] Moore L S and Goldhaber-Gordon D 2007 Magnetic lattice surprise *Nat. Phys.* **3** 295–296

[11] Wiesendanger R 2016 Nanoscale magnetic skyrmions in metallic films and multilayers: A new twist for spintronics *Nat. Rev. Mater.* **1** 16044

[12] Salaheldeen M, Vega V, Ibabe A, Jaafar M, Asenjo A, Fernandez A and Prida V M 2018 Tailoring of Perpendicular Magnetic Anisotropy in Dy13Fe87 Thin Films with Hexagonal Antidot Lattice Nanostructure *Nanomaterials* **8** 227

[13] Fukuda H M and K 1995 Ordered Metal Nanohole Arrays Made by a Two-Step Replication of Honeycomb Structures of Anodic Alumina *Science.* **268** 1466

[14] Shaban M, Ahmed A M, Abdel-Rahman E and Hamdy H 2014 Fabrication and characterization of micro/nanoporous Cr film for sensing applications *Microporous Mesoporous Mater.* **198** 115–21

[15] Salaheldeen M, Vega V, Caballero-Flores R, Prida V M and Fernández A 2019 Influence of nanoholes array geometrical parameters on magnetic properties of Dy-Fe antidot thin films *Nanotechnology* **30** 455703

[16] Shaban M, Hamdy H, Shahin F and Ryu S W 2010 Strong surface plasmon resonance of ordered gold nanorod array fabricated in porous anodic alumina template *J. Nanosci. Nanotechnol.* **10** 3034–7

[17] Krupinski M, Mitin D, Zarzycki A, Szkudlarek A, Giersig M, Albrecht M and Marszałek M 2017 Magnetic transition from dot to antidot regime in large area Co/Pd nanopatterned arrays with perpendicular magnetization *Nanotechnology* **28** 085302

[18] Saldanha D R, Dugato D A, Mori T J A, Daudt N F, Dorneles L S and Denardin J C 2018 Tailoring the magnetic and magneto- transport properties of Pd / Co multilayers and pseudo-spin valve antidots *J. Phys. D. Appl. Phys.* **51** 395001

[19] Wiedwald, U.; Gräfe, J.; Lebecki, K. M.; Skripnik, M.; Haering, F.; Schütz, G.; Ziemann, P.; Goering, E.; Nowak U 2016 Magnetic switching of nanoscale antidot lattices *Beilstein J. Nanotechnol.* **7** 733–750

[20] Béron F, Kaidatzis A, Velo M F, Arzuza L C C, Palmero E M, del Real R P, Niarchos D, Pirota K R and García-Martín J M 2016 Nanometer Scale Hard/Soft Bilayer Magnetic Antidots *Nanoscale Res. Lett.* **11** 1–11

[21] Jang Y H and Cho J H 2014 Morphology-dependent multi-step ferromagnetic reversal processes in Co thin films on crescent-shaped antidot arrays *J. Appl. Phys.* **115** 063903

[22] Liu X M, Ding J and Adeyeye A O 2012 Magnetization dynamics and reversal mechanism of Fe filled Ni 80Fe 20 antidot nanostructures *Appl. Phys. Lett.* **100** 242411

[23] Merazzo K J, Castán-Guerrero C, Herrero-Albillos J, Kronast F, Bartolomé F, Bartolomé J, Sesé J, Del Real R P, García L M and Vázquez M 2012 X-ray photoemission electron microscopy studies of local magnetization in Py antidot array thin films *Phys. Rev. B - Condens. Matter Mater. Phys.* **85** 184427

[24] Castán-Guerrero C, Bartolomé J, Bartolomé F, García L M, Sesé J, Strichovanec P, Herrero-Albillos J, Merazzo K J, Vázquez M and Vavassori P 2013 Coercivity dependence on periodicity of Co and Py antidot arrays *J. Korean Phys. Soc.* **62** 1521–4

[25] Castán-Guerrero C, Herrero-Albillos J, Bartolomé J, Bartolomé F, Rodríguez L A, Magén C, Kronast F, Gawronski P, Chubykalo-Fesenko O, Merazzo K J, Vavassori P, Strichovanec P, Sesé J and García L M 2014 Magnetic antidot to dot crossover in Co and Py nanopatterned thin films *Phys. Rev. B - Condens. Matter Mater. Phys.* **89** 144405

[26] Fettar F, Cagnon L and Rougemaille N 2010 Three-dimensional magnetization profile and multiaxes exchange bias in Co antidot arrays *Appl. Phys. Lett.* **97** 192502

[27] Nguyen, T. N. A.; Fedotova, J.; Kasiuk, J.; Bayev, V.; Kupreeva, O.; Lazarouk, S.; Manh, D. H.; Vu, D. L.; Chung, S.; Akerman, J.; Altynov, V.; Maximenko A 2018 Effect of flattened surface morphology of anodized aluminum oxide templates on the magnetic properties of nanoporous Co / Pt and Co / Pd thin multilayered films *Appl. Surf. Sci.* **427** 649–55

[28] Gawronski P, Merazzo K J, Chubykalo-Fesenko O, Del Real R P and Vázquez M 2014 Micromagnetism of permalloy antidot arrays prepared from alumina templates *Nanotechnology* **25** 475703

[29] Navas D, Hernández-V́lez M, Vázquez M, Lee W and Nielsch K 2007 Ordered Ni nanohole arrays with engineered geometrical aspects and magnetic anisotropy *Appl. Phys. Lett.* **90** 192501

[30] Lambert C H, Rajanikanth A, Hauet T, Mangin S, Fullerton E E and Andrieu S 2013 Quantifying perpendicular magnetic anisotropy at the Fe-MgO(001) interface *Appl.*

Phys. Lett. **102** 2410–5

[31] Shaw J M, Russek S E, Thomson T, Donahue M J, Terris B D, Hellwig O, Dobisz E and Schneider M L 2008 Reversal mechanisms in perpendicularly magnetized nanostructures *Phys. Rev. B - Condens. Matter Mater. Phys.* **78** 024414

[32] Yanagishita T, Nishio K and Masuda H 2005 Fabrication of metal nanohole arrays with high aspect ratios using two-step replication of anodic porous alumina *Adv. Mater.* **17** 2241–3

[33] Merazzo K J, Leitao D C, Jiménez E, Araujo J P, Camarero J, Del Real R P, Asenjo A and Vázquez M 2011 Geometry-dependent magnetization reversal mechanism in ordered Py antidot arrays *J. Phys. D. Appl. Phys.* **44** 5001–10